East European Journal of Physics. **4.** 216-225 (2023)
DOI:10.26565/2312-4334-2023-4-27 ISSN 2312-4334

NUMERICAL STUDY OF T-GATE AlGaN/AlInGaN/GaN MOSHEMT WITH SINGLE AND DOUBLE BARRIER FOR THZ FREQUENCY APPLICATIONS

Amina Noual[a], Messai Zitouni[b], Zine-eddine Touati[b], Okba Saidani[b], Abderrahim Yousfi[b]*
[a] *LIST Laboratory, University of M'Hamed Bougara, Boumerdes, Algeria*
[b] *ETA Laboratory, Department of electronics, Faculty of technology, University Mohamed El Bachir El Ibrahimi of Bordj Bou Arréridj-34030, Algeria*
**Corresponding Author e-mail: Abderrahim.yousfi@univ-bba.dz*
Received October 1, 2023; revised October 16, 2023; accepted November 5, 2023

This paper presents a comprehensive investigation into the DC analog and AC microwave performance of a state-of-the-art T-gate double barrier AlGaN/AlInGaN/GaN MOSHEMT (Metal Oxide Semiconductor High Electron Mobility Transistor) implemented on a 4H-SiC substrate. The study involves meticulous numerical simulations and an extensive comparison with a single barrier design, utilizing the TCAD-Silvaco software. The observed disparity in performance can be attributed to the utilization of double barrier technology, which enhances electron confinement and current density by augmenting the polarization-induced charge during high-frequency operations. Remarkably, when compared to the single barrier design, the double barrier MOSHEMT exhibits a notable 15% increase in drain current, a 5% increase in transconductance, and an elevated breakdown voltage (VBR) of 140 V in E-mode operation. Furthermore, the radio frequency analysis of the double barrier device showcases exceptional performance, setting new records with a maximum oscillation frequency (fmax) of 1.148 THz and a gain cutoff frequency (ft) of 891 GHz. These impressive results obtained through deck-simulation affirm the immense potential of the proposed double barrier AlGaN/AlInGaN/GaN MOSHEMT for future applications in high-power and terahertz frequency domains.
Key words: *TiO_2-MOSHEMT; T-gate; Double barrier; AlInGaN Quaternary material; Maximum THz frequency; TCAD-Silvaco*
PACS: 73.40.–c, 85.30.Pq

1. INTRODUCTION

The emerging generation of power switching circuits has garnered significant attention due to the impressive capabilities of AlGaN/GaN HEMTs (High Electron Mobility Transistors) in facilitating high power and high-frequency operations. These HEMTs are poised to find applications in diverse fields such as 5G technology, sensors, automotive systems, defense, and space communications [1, 2]. The exceptional performance of AlGaN/GaN HEMTs can be attributed to the presence of a high-mobility two-dimensional electron gas (2DEG) formed and accumulated at the AlGaN/GaN interface, resulting from a strong sheet polarization charge effect [3]. To reduce gate leakage current and enhance performance, a MOS (Metal Oxide Semiconductor) HEMT heterostructure is employed by introducing an oxide layer at the intersection of the gate electrode and AlGaN barrier. Various gate oxide materials, such as TiO_2, HfO_2, Al_2O_3, SiO_2, and Si_3N_4, are commonly used in MOSHEMT transistors [4-7]. Conventionally, GaN-based HEMTs operate in a depletion mode (normally-on operation) since the 2DEG is present at the heterointerface even without gate polarization. However, enhancement mode functionality is preferred to reduce production charge, simplify digital circuits, and enhance safety. Multiple technological approaches have been proposed to achieve normally-off behavior [8-10]. One novel approach, initially suggested by Ketteniss et al. and subsequently confirmed, involves using a thin quaternary AlInGaN barrier layer that introduces polarization engineering between the barrier and the GaN channel, enabling E-mode operation [11, 12]. Quaternary nitride has garnered significant attention as an alternative to AlGaN barrier layers due to its promising DC and RF performance, including the ability to utilize high aluminum content, leading to increased spontaneous polarization induced by high 2DEG carrier density ($n_s > \sim 1.8\times10^{13}$ cm^{-2}) and high mobility ($\mu > \sim 1800$ cm^2/V s) [13-15]. Traditionally, since 1991, HEMT transistors have been designed and fabricated with a single barrier layer [16]. However, in 1999, Gaska et al. first demonstrated a double AlGaN barrier structure [17]. Subsequently, various designs featuring $Al_{x1}Ga_{y1}N/Al_{x2}Ga_{y2}N$/GaN double heterojunctions have been explored theoretically and experimentally, showcasing high current and high-frequency performance due to enhanced carrier confinement properties and higher 2DEG density [18-20]. Moreover, recent investigations have focused on bilayer barrier structures with quaternary alloys, resulting in the development of an $Al_{x1}In_{y1}Ga_{z1}N/Al_{x2}In_{y2}Ga_{z2}N$/GaN HEMT with high current density [21, 22]. However, to date, most experimental and theoretical studies have focused on dual AlGaN or double AlInGaN barrier-based HEMTs, with limited optimization efforts targeting the DC and RF properties of an AlGaN/AlInGaN/GaN double heterostructure.

In this study, we propose, for the first time, an E-mode $Al_{0.30}Ga_{0.70}N$ / $Al_{0.80}In_{0.18}Ga_{0.02}N$/GaN MOSHEMT with a double barrier structure, incorporating an ultra-thin quaternary spacer layer ($Al_{0.36}In_{0.08}Ga_{0.56}N$). The proposed design aims to enhance electron accumulation in the channel and improve radio frequency performance, extending it into the terahertz regime. To analyze and optimize the structure, we employed the Silvaco-Atlas software, enabling a thorough investigation of the proposed double barrier MOSHEMT and a comparison with a single barrier $Al_{0.30}Ga_{0.70}N$/GaN MOSHEMT design.

Cite as : A. Noual, Z. Messai, Z. Touati, O. Saidani, A. Yousfi, East Eur. J. Phys. 4, 216 (2023), https://doi.org/10.26565/2312-4334-2023-4-27

2. DEVICE SETTINGS AND SIMULATION PROCESS

Figure 1 presents a comprehensive 3D view of the proposed GaN-MOSHEMT transistor. The device parameters utilized in this study are listed in Table 1. To enhance the device's characteristics, T-gate technology is employed, allowing for a short gate length of 10nm (corresponding to the base of the T-shape) [23]. Examining the heterostructure design from top to bottom, a Silicon dioxide (SiO2) passivation layer is implemented to minimize surface traps. Underneath the source and drain regions, a two-graded, heavily doped n++ GaN layer with $2\times10^{19}cm^{-3}$ donors is regrown to minimize access resistance [24]. An oxide layer comprising high-k Titanium dioxide (TiO_2) with a dielectric constant (k) of 80 is deposited beneath the gate electrode. Research has shown that employing a TiO_2 oxide layer facilitates high off-state breakdown voltage and reduced current losses, thereby enabling E-mode operation [25, 26]. A thin (2nm) GaN cap layer follows the oxide layer. The heterostructure continues with a non-doped AlGaN first barrier layer featuring a 30% aluminum concentration, positioned under the GaN cap. The conventional composition (x) of the ternary alloy leads to material relaxation. To further enhance the device's performance, a thin $Al_{0.36}In_{0.08}Ga_{0.56}N$ spacer layer is inserted between the GaN channel and the AlGaN barrier. Recent research indicates that the 2DEG-charge at the $Al_xIn_yGa_zN$/GaN interface (associated with the $Al_xIn_yGa_zN$ thin spacer layer) is greater than that at the AlN/GaN interface (related to the AlN spacer layer). This is attributed to the induction of a high polarization charge, resulting in improved mobility and current flow through the region [21, 27]. Therefore, a quaternary material, $Al_{0.36}In_{0.08}GaN$, is employed as the spacer layer. To further optimize 2DEG confinement in the channel region, an Al0.80In0.18GaN second barrier layer with high aluminum/indium content is placed between the AlGaN first barrier and the $Al_{0.36}In_{0.08}GaN$ spacer (as shown in Figure 1(b)). The calculated Al, In, and Ga composition for the AlInGaN materials ensures lattice-matching with the GaN channel, promoting superior transport performance [28]. These studied structures are grown on a preferred substrate of silicon carbide (4H-SiC). Nanjo et al. have confirmed that the 4H-SiC epitaxial substrate outperforms sapphire substrates, primarily due to its excellent thermal stability [29]. Referring to Figure 1(a) and Figure 1(b), the single barrier device is designated as STR01-SB, while the double barrier device is designated as STR02-DB.

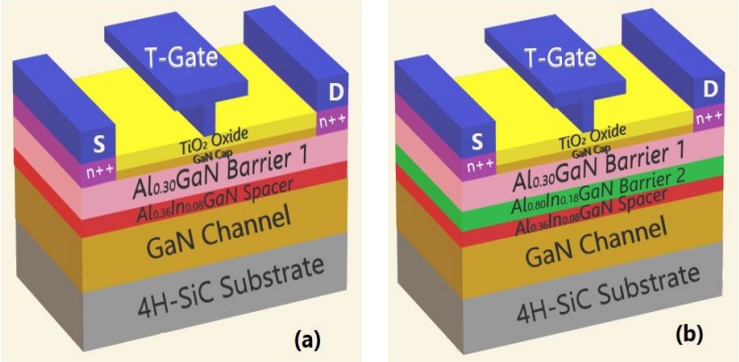

Figure 1. 3D view design of a 10nm T-gate (a) Single barrier $Al_{0.30}Ga_{0.70}N$ / $Al_{0.36}In_{0.08}Ga_{0.56}N$ / GaN MOSHEMT, (b) Double barrier $Al_{0.30}Ga_{0.70}N$ / $Al_{0.80}In_{0.18}Ga_{0.02}N$ / Al0.36$In_{0.08}Ga_{0.56}N$ / GaN MOSHEMT

Table 1. Geometrical specifications of the studied device with single and double barrier.

Gate specifications		**Structure specifications**		
Parameter	**Dimension**	**Layer**	**STR01-SB**	**STR02-DB**
Gate structure	T-shape	**TiO_2 oxide layer**	5 nm	5 nm
Gate foot length	10 nm	**GaN cap layer**	2 nm	2 nm
Gate head length	400 nm	**$Al_{0.30}GaN$ 1st barrier**	20 nm	20 nm
Gate stem height	50 nm	**$Al_{0.80}In_{0.18}GaN$ 2st barrier**	--	4 nm
Gate-drain distance	355 nm	**$Al_{0.36}In_{0.08}GaN$ spacer**	2 nm	2 nm
Gate-source distance	355 nm	**GaN channel**	796 nm	796 nm
Gate work function	5.93	**4H-SiC substrate**	2165 nm	2161 nm

The electrical parameters of the suggested MOSHEMT transistor are evaluated using a physical model of 2D-TCAD simulation at 300k, the fundamental model used for all semiconductor device is the Drift-Diffusion model; by resolving the Poisson and electron/hole continuity equations. It computes at each moment and any point of the structure the concentration of electrons and the value of the potential. Shockley-Read Hall recombination/generation model, field-dependent mobility model, and polarization model are applied as additional physical models in the deck-simulation. Selberherr's impact ionization model is considered for device breakdown simulation. These physical models are resolved using the numerical Newton's method [30, 31]. The electrical characteristics of the proposed MOSHEMT transistor were assessed through a rigorous evaluation utilizing a 2D-TCAD simulation based on physical models. This evaluation was conducted at a temperature of 300 K. The Drift-Diffusion model, which is widely used for semiconductor devices, was employed as the fundamental model. By solving the Poisson equation and the electron/hole continuity equations, this model determines the concentration of electrons and the potential values at any given point and time within the structure.

In addition to the Drift-Diffusion model, several other physical models were incorporated into the simulation to enhance its accuracy. The Shockley-Read Hall recombination/generation model, which accounts for recombination and generation of charge carriers, was utilized. Furthermore, a field-dependent mobility model and a polarization model were applied to accurately capture the device behavior under different electric fields. To simulate the breakdown behavior of the device, Selberherr's impact ionization model was employed. This model provides insights into the phenomenon of impact ionization, which can lead to device breakdown under certain conditions.

The bandgap energy of Al_xGa_zN and $Al_xIn_yGa_zN$ materials is dependent on the composition of mole fraction x, y and z, using Vegard's Law, it can be expressed as a sum of the bandgap energies of GaN, InN and AlN binary semiconductors with appropriate bowing parameters [21, 25]. $Al_xIn_yGa_zN$ alloy offers an additional degree of freedom in the bandgap mole fraction ratio where x+ y + z = 1 compared with Al_xGa^zN, where x + z = 1. Equations (1) and (2) describe their expressions:

$$E_g^{Al_xGa_{1-x}N} = xE_g^{AlN} + zE_g^{GaN}, \tag{1}$$

$$E_g^{Al_xIn_yGa_zN} = xE_g^{AlN} + yE_g^{GaN} + zE_g^{InN} - xy(1-z)b_{AlInN} - yz(1-x)b_{InGaN}. \tag{2}$$

The following equations provide the dielectric constant for ternary and quaternary alloys as a function of alloy composition:

$$\varepsilon_{Al_xGa_zN} = 8.5x + 8.9x, \tag{3}$$

$$\varepsilon_{Al_xIn_yGa_zN} = 8.5x + 15.3y + 8.9z. \tag{4}$$

The creation of a large 2D electron gas density in the heterojunction is the most important operation of the charge polarization property. For sample I (STR01-SB), two negative polarization-induced charges are present at the $Al_{0.30}Ga_{0.70}N/Al_{0.36}In_{0.08}Ga_{0.56}N$ interface and $Al_{0.36}In_{0.08}Ga_{0.56}N/GaN$ interface (noted σ′1 and σ′2, respectively). Thanks to a lattice-matched between the AlInGaN material and the GaN channel, the piezoelectric polarization effect is neglected. Therefore, the total polarization σ'_{int} is a function of spontaneous polarization (Psp) as $\sigma'_{int} = \sigma'1 + \sigma'2$ with:

$$\sigma'' = P_{sp}(Al_{0.08}In_{0.18}Ga_{0.02}N) - P_{sp}(Al_{0.30}Ga_{0.70}N), \tag{5}$$

$$\sigma_2'' = P_{sp}(Al_{0.36}In_{0.08}Ga_{0.56}N) - P_{sp}(Al_{0.80}In_{0.18}Ga_{0.02}N), \tag{6}$$

$$\sigma'' = P_{sp}(Al_{0.08}In_{0.18}Ga_{0.02}N) - P_{sp}(Al_{0.30}Ga_{0.70}N). \tag{7}$$

The mathematical equations of the spontaneous polarization of the ternary and quaternary alloys is mentioned in equations (8) and (9), the details is reported in [32, 33].

$$P_{sp}^{AlGaN} = xP_{sp}^{AlN} - zP_{sp}^{GaN} + xzb_{AlGaN}, \tag{8}$$

$$P_{sp}^{AlInGaN} = xP_{sp}^{AlN} + yP_{sp}^{InN} + zP_{sp}^{GaN} + xzb_{AlGaN} + yzb_{InGaN} + xyb_{AlInN}. \tag{9}$$

According to equations (8) and (9), AlInGaN material has a higher spontaneous polarization due to the additional contribution of the spontaneous polarization and the bowing parameter corresponding to indium content, which enhances the 2DEG concentration and the charge carrier density. The calculated polarization of both structures at the active interfaces are displayed in Fig.2.

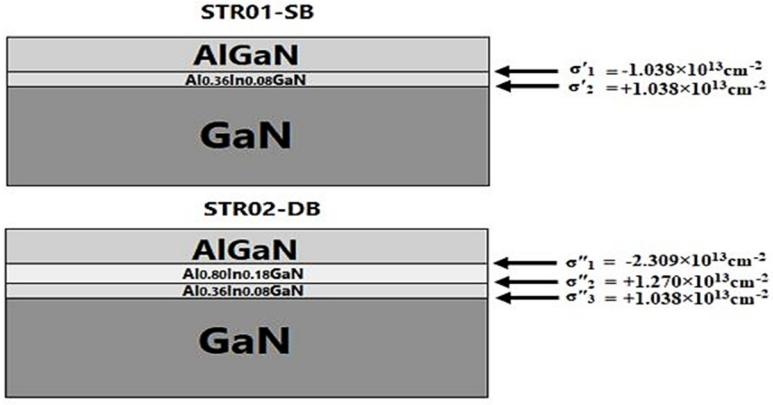

Figure 2. Polarization interface charge of both STR01-SB and STR02-DB.

The sheet charge density ns of AlGaN and AlInGaN alloys is a function of interface polarization-induced charge σint and the conduction band offset ΔE_c [34], as indicated in equations (10) and (11):

$$n_s^{AlGaN} = \frac{\sigma_{int}(x)}{q} - \frac{\varepsilon_0 \varepsilon(x)\left[q\varnothing_b(x) + E_F + \Delta E_c(x)\right]}{q^2 d}, \tag{10}$$

$$n_s^{AlInGaN} = \frac{\sigma_{int}(x,y)}{q} - \frac{\varepsilon_0 \varepsilon(x,y)\left[q\varnothing_b(x,y) + E_F + \Delta E_c(x,y)\right]}{q^2 d}. \tag{11}$$

Where d is the barrier thickness, ε is the barrier's dielectric constant, $\varnothing_b$ is the Schottky barrier of gate contact and E_F is the Fermi energy level. The main physical parameters of the several materials extracted during the simulation are shown in Table 2.

Table 2. The extracted physical parameters used in this work at 300k

Material	Al0.30GaN	Al0.80In0.18GaN	Al0.36In0.08GaN	GaN
Permittivity ε	8.9	9.73	9.27	9.5
Band gap Eg (eV)	3.42	4.55	3.71	3.55
Electron density of state Ec (×1018cm-3)	2.02	3.01	2.45	1.07
Hole density of state Ev (×1019cm-3)	9.08	3.30	2.10	1.16
Electron mobility μe(cm2/V.s)	985.5	1280	1280	1350
Spontaneous polarization Psp (×1013cm-3)	-1.698	-4.007	-2.736	-1.698
Doping layer (×1018cm-3)	00	02	03	00

3. RESULTS AND DISCUSSION

Figure 3(a) depicts the conduction and valence band discontinuity offset in the proposed heterojunction under unbiased conditions (off-state). The AlInGaN and GaN layers exhibit a difference in their band gaps, leading to an accumulation of electrons in the quantum well and the formation of a two-dimensional electron gas at the interface of the spacer and channel. By incorporating a second barrier layer, a significant conduction band offset and higher sheet polarization density are achieved, resulting in a greater depth of the quantum well below the Fermi level. Numerical simulations indicate that the sheet density of the two-dimensional electron gas is measured at 4.97×10^{12} cm^{-2} for STR02-DB, whereas it is 2.3×10^{12} cm^{-2} for STR01-SB. Additionally, the extrinsic peak of electron concentration increases, reaching approximately 1.2×10^{19} cm^{-2} for sample I and 2.5×10^{19} cm^{-2} for sample II, as illustrated in Figure 3(b).

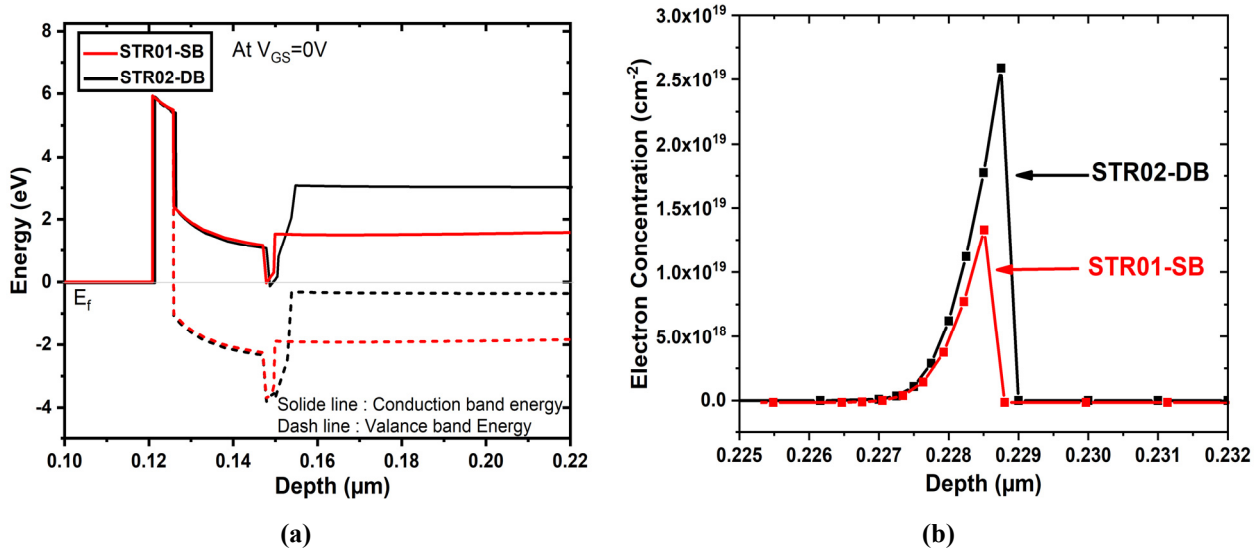

Figure 3. (a) Conduction and valence band diagram (b) Electron concentration of the studied device with single and double barrier at zero gate bias

3.1. DC results

This section presents the DC results of the TiO_2-based MOSHEMT (Metal-Oxide-Semiconductor High Electron Mobility Transistor) with single and double barriers, including output characteristics, ON-resistance, transfer characteristics, threshold voltage, Ion/Ioff ratio, and transconductance. Table 3 provides an overview of the DC performance metrics of the recommended nano-MOSHEMT.

Table 3. Comparison of the DC results of STR01-SB and STR02-DB

Parameters	Units	Values	
		STR01-SB	STR02-DB
ID,max	mA/mm	3300	3780
Ron	Ω.mm	5.4	3.9
Vth	V	+ 2.8	+ 3.2
Gm, max	mS/mm	4320	4470

Figure 4 illustrates the drain current as a function of drain voltage at different gate-source voltages (VGS = 1, 2, and 3 V). The maximum drain saturation current (ID, max) for STR01-SB and STR02-DB was observed at 3300 and 3780 mA/mm, respectively, at VGS = 3 V and VDS = 8 V. Notably, the utilization of a high aluminum composition in both the first barrier (x = 30%) and the second AlInGaN barrier (x = 80%) along with an ultrashort gate length (Lg = 10 nm) significantly enhances the drain current density. STR02-DB exhibits approximately a 15% increase in ID, max compared to the STR01-SB device. The ON-resistance (Ron) is determined from the linear region of the drain current and is found to be 5.4 and 3.9 Ω.mm for STR01-SB and STR02-DB, respectively.

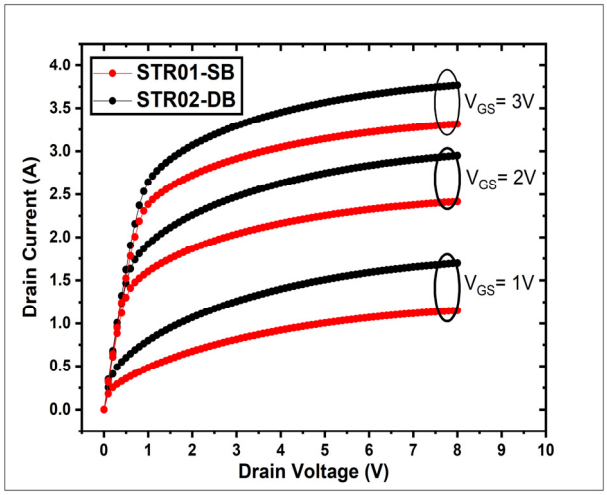

Figure 4. ID-VD characteristics of the simulated GaN MOSHEMT with single and double barrier

In Figure 5(a), the I-V input characteristics at VDS = 3V are presented. A threshold voltage (Vth) of +2.8 V and +3.2 V was extracted for sample I and II, respectively, from the linear scale plot. The transistor operates in the enhancement mode (E-mode).

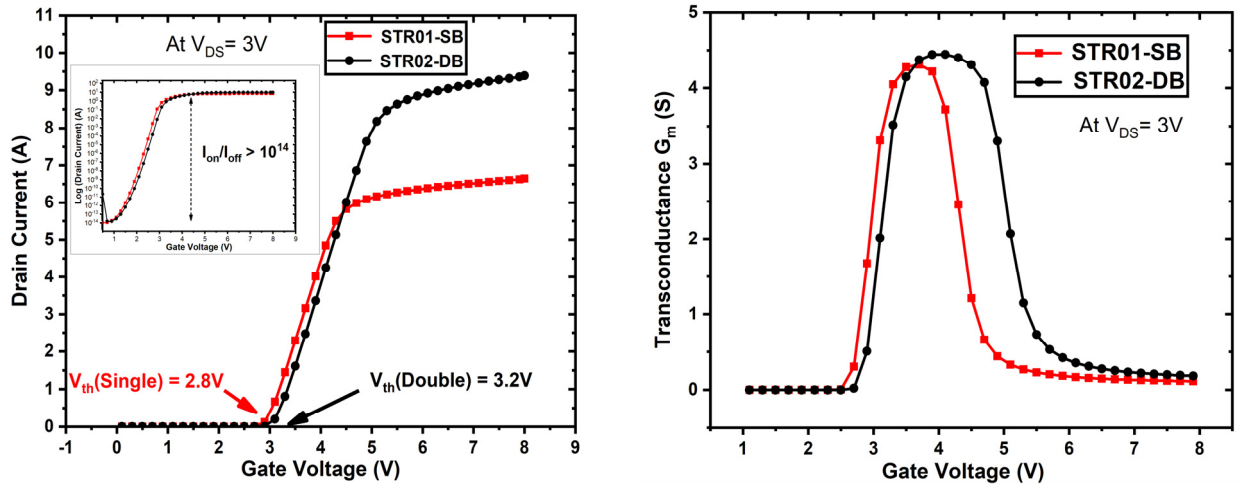

Figure 5. Transfer characteristics of the proposed nano-MOSHEMT at VDS = 3 V, (a) ID-VG in a linear scale, inset ID -VG in log scale, showing the Ion/Ioff ratio, (b) Transconductance Gm

The positive shift in Vth can be attributed to the utilization of the TiO_2 insulating layer and the activated interface charge of 1.85×10^{13} cm^{-2} donors at the oxide/semiconductor interface. This negative charge accumulates at the TiO_2/GaN interface, depleting the 2DEG charge and causing Vth to shift more positively. The inset of Figure 5(a) displays the logarithmic-scale plot of ID-VG, showing an Ion/Ioff ratio larger than 10^{14}, indicating exceedingly low drain leakage

current in the proposed heterostructure. Figure 5(b) shows the variation of transconductance (Gm) as a function of VGS, calculated from the derivative of the ID-VGS curve at a fixed VDS. Sample II exhibits a high peak extrinsic transconductance of ~ 4470 mS/mm, while sample I demonstrates 4320 mS/mm, both at VGS ~ 4 V and VDS = 3 V. The significant Gm values can be attributed to the excellent interface charge-induced strong controllability of the very short gate, enabling high-frequency performance. Overall, the suggested 10nm T-gate double barrier $Al_{0.30}Ga_{0.70}N/Al_{0.80}In_{0.18}Ga_{0.02}N/Al_{0.36}In_{0.08}Ga_{0.56}N$/GaN MOSHEMT demonstrates superior performance in terms of ID, Ron, and Gm for achieving normally-off operation.

3.2. Breakdown voltage

Figure 6 presents the breakdown voltage characteristics of the proposed nano-MOSHEMT. In high-power millimeter-wave applications, the breakdown voltage (VBR) of the transistor plays a critical role and is primarily influenced by the impact ionization phenomenon. To enhance the VBR profiles in the suggested heterojunctions, a short symmetric T-gate shape is employed. According to the Selberherr's model simulation, the off-state breakdown voltage for STR01-SB and STR02-DB is significantly improved. The breakdown voltage is measured at 126 V for STR01-SB and 140 V for STR02-DB. It is worth noting that employing a single barrier MOSHEMT results in a 10% decrease in breakdown voltage compared to the double barrier device. This reduction in breakdown voltage is clearly illustrated in Figure 6. Overall, the implementation of a short symmetric T-gate shape contributes to the enhancement of breakdown voltage profiles in the suggested heterojunctions, making them well-suited for high-power millimeter-wave applications.

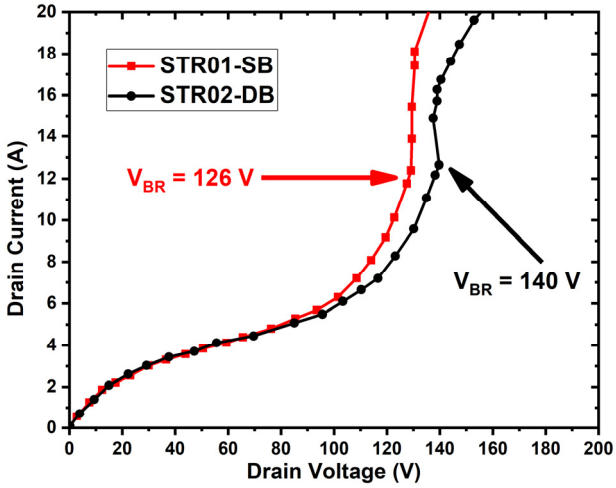

Figure 6. Off-state breakdown voltage simulation results

3.3. Microwave results

In this section, an investigation of the AC and RF characteristics has been conducted for the proposed device with single and double barriers. The simulation results are presented in Figures 7, 8, and 9.

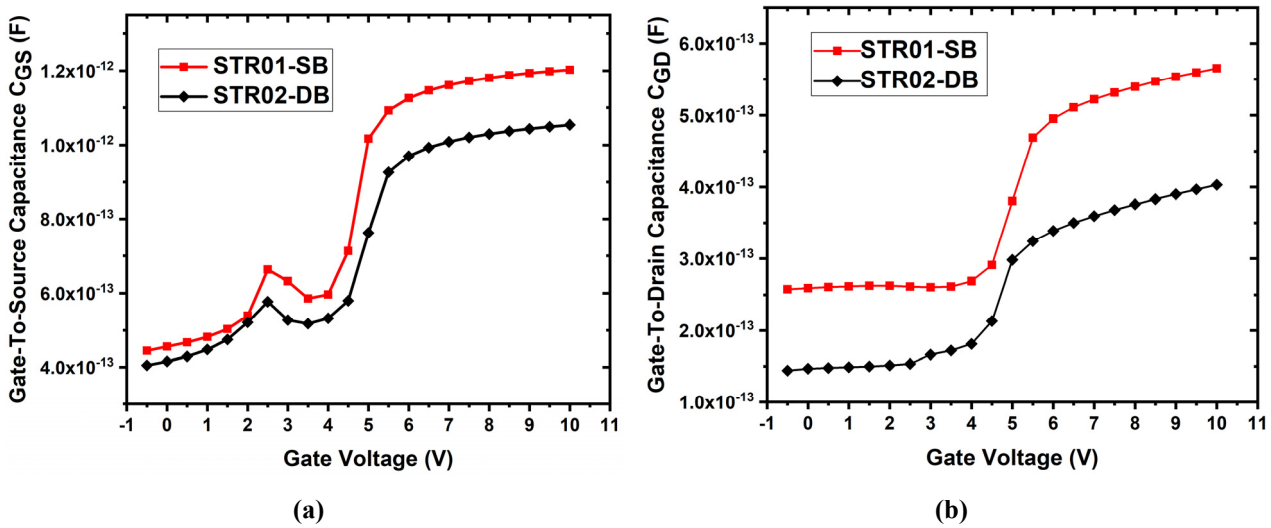

Figure 7. C-V Characteristics of the simulated devices (a) Gate-to-source capacitance (CGS),(b) Gate-to-drain capacitance (CGD)

To analyze the capacitance-voltage characteristics of the simulated devices, measurements were performed at a frequency of 1 MHz. Figure 7(a) and (b) illustrate the variation of the gate-to-source capacitance (CGS) and gate-to-drain capacitance (CGD) as a function of gate-to-source voltage (VGS) at a fixed drain-to-source voltage (VDS) of 5 V. The total gate capacitance, CG, is defined as the sum of CGS and CGD. It is observed that the bilayer device exhibits a lower total gate capacitance, CG, of 1.453 pF compared to 1.767 pF for the single barrier design. This reduction in total gate capacitance indicates improved performance in terms of capacitive effects, which can have a positive impact on high-frequency operation. For future generation of millimeter and terahertz spectrum applications, ft and fmax are figures of merit in radio frequency performances [35-37]. Mathematically, they expressed as follows:

$$f_t = \frac{G_m}{2\pi(C_{GS} + C_{GD})} \tag{12}$$

$$f_{\max} = \frac{f_t}{2\sqrt{C_{DS}(R_G + R_S) + 2\pi f_t (R_G C_{GD}}} \tag{13}$$

From equation (12), ft is proportional to Gm and inversely related to CG. Thus, the gate voltage at the maximum Gm should be used as the gate polarization to approximate ft and fmax. Equation (13) demonstrates that fmax is influenced by ft and other factors (where GDS represents drain-to-source conductance and RS, RG stand for source and gate resistance, respectively).The cutoff frequency and the maximum oscillation frequency referred to the frequencies when the curves of the current gain H21 and the power gain Ug are unity [38]. Their expressions in relation to S-parameters is described in equations (14) and (15):

$$H_{21} = \left| \frac{-2S_{21}}{(1 - S_{11})(2 - S_{22}) - (S_{12}S_{21})} \right| \tag{14}$$

$$U_g = \frac{|S_{21}|^2}{(1 - |S_{11}|^2)(1 - |S_{22}|^2)} \tag{15}$$

Based on TCAD simulation, the key RF parameters of the considered device, namely the transit frequency (ft) and the maximum oscillation frequency (fmax), were extracted and are depicted in Figure 8(a) and (b).

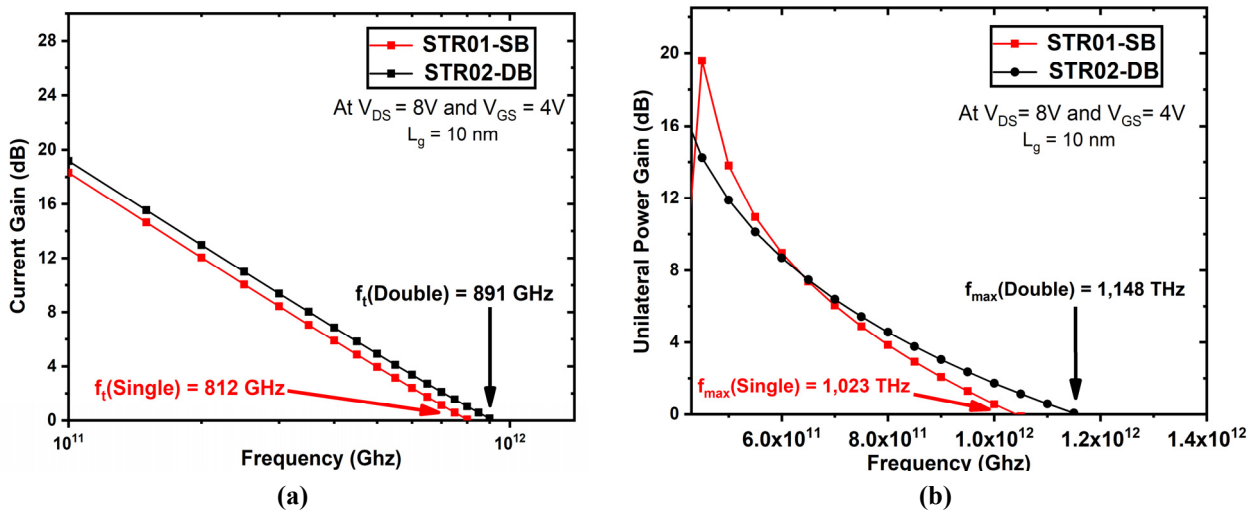

Figure 8. Small signal characteristics with single and double barrier at VGS = 4 V, VDS = 8 V, (a) Current gain, (b) Unilateral power gain

The measurements were conducted at a drain-to-source voltage (VDS) of 8 V and a gate-to-source voltage (VGS) of 4 V, corresponding to the peak transconductance (Gm). Remarkably, the achieved ft/fmax values for STR01-SB and STR02-DB are 812/1023 GHz and 891/1148 GHz, respectively. These represent new records for the highest ft/fmax reported to date in quaternary barrier devices. The superior ft/fmax performance can be attributed to the utilization of a symmetric 10 nm T-gate structure, a TiO_2 oxide layer, and a thin quaternary spacer layer.

Figure 9 showcases the optimization of the output current gain and power gain for the proposed AlGaN/AlInGaN/GaN MOSHEMT at different gate lengths (Lg = 10, 20, 35, 50 nm). Through simulation analysis, it is evident that the device with an ultrashort gate length exhibits excellent RF efficiency, along with the highest fmax achieved among quaternary barrier devices reported thus far. Notably, as the gate length (Lg) decreases, ft and fmax gradually increase. This behavior can be attributed to the reduction in both CGS and CGD capacitances. According to Equations (14) and (15), ft and fmax exhibit steady growth as the gate capacitance decreases. Therefore, when designing

E-mode GaN MOSHEMTs, it is advisable to reduce the gate length while considering the technological limitations. The proposed design, featuring a 10 nm T-shaped gate in both single and double barrier III-nitride MOSHEMTs grown on a 4H-SiC substrate, demonstrates superior microwave performance compared to recent research works. These ft and fmax values set new records for GaN-based MOSHEMTs in terms of high-speed power and terahertz frequency operations. The main electrical characteristics obtained from the proposed MOSHEMT are summarized and compared with previous experimental results in Table 4, highlighting its favorable performance.

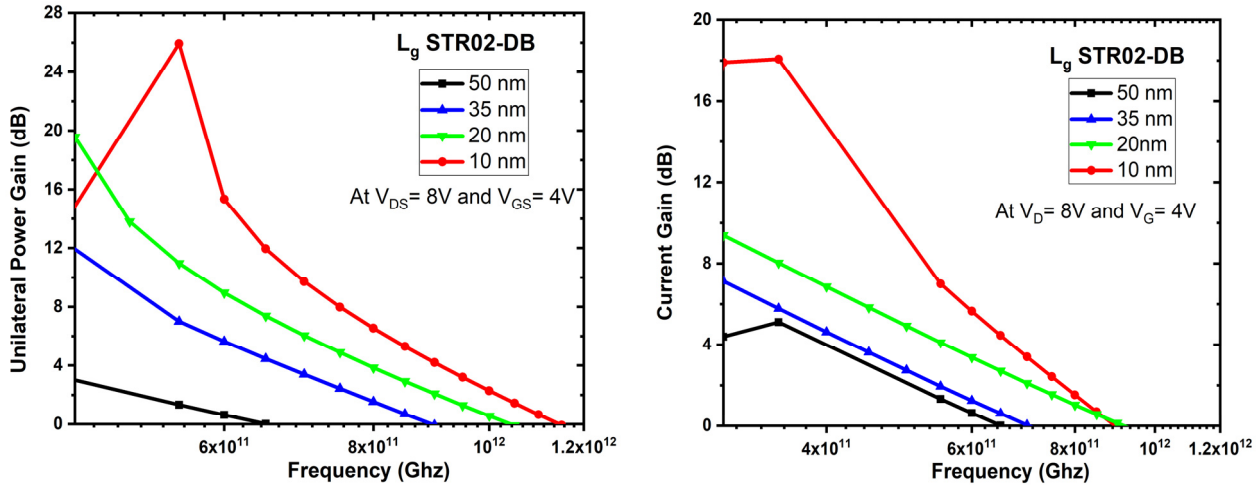

Figure 9. Small signal characteristics of double barrier GaN-based MOSHEMT with respect of T-gate length (Lg = 10, 20, 35, and 50 nm) (a) Current gain, (b) Unilateral power gain

Table 4. Performance comparison of our results with similar experimental reports

Ref	Transistor Device	ns×10^{13} cm^{-2}	ID A	Vth V	Gm mS	VBR V	CG pF	ft GHz	fmax GHz
[18], 2020	Al0.30GaN/Al0.20GaN/ GaN	--	--	0	68.9	--	220	--	--
[39], 2015	Al0.85In0.10GaN/ Al0.15GaN/AlN/GaN	3.5	0.73	+1.1	--	--	--	--	--
[22], 2019	Al0.54In0.12GaN/ Al0.18In0.04GaN /GaN	--	0.76	+0.4	493	--	--	--	--
[21], 2020	Al0.72In0.16GaN/ Al0.18In0.04GaN/ Al0.80In0.18GaN /GaN	1.2	0.11	+0.2	358	--	--	--	--
[40], 2022	Al0.165In0.775GaN/ Al0.60GaN /GaN	1.6	0.2	-1.5	--	--	38	0.95	4.5
[14], 2019	$Al_{0.74}In_{0.16}GaN/AlN/GaN/Al_{0.08}GaN$	1.81	2.9	-2.8	900	38	0.275	310	425
This work	STR 01-SB	0.23	3.30	+2.8	4320	126	1.767	812	1023
	STR 02-DB	0.49	3.78	+3.2	4470	140	1.453	891	1148

4. CONCLUSION

In summary, this study presents a comprehensive investigation into the DC analog and AC microwave performance of a state-of-the-art T-gate double barrier AlGaN/AlInGaN/GaN MOSHEMT (Metal Oxide Semiconductor High Electron Mobility Transistor) implemented on a 4H-SiC substrate. The study involves meticulous numerical simulations and an extensive comparison with a single barrier design, utilizing the TCAD-Silvaco software. The observed disparity in performance can be attributed to the utilization of double barrier technology, which enhances electron confinement and current density by augmenting the polarization-induced charge during high-frequency operations. Remarkably, when compared to the single barrier design, the double barrier MOSHEMT exhibits a notable 15% increase in drain current, a 5% increase in transconductance, and an elevated breakdown voltage (VBR) of 140 V in E-mode operation. Furthermore, the radio frequency analysis of the double barrier device showcases exceptional performance, setting new records with a maximum oscillation frequency (fmax) of 1.148 THz and a gain cutoff frequency (ft) of 891 GHz. These impressive results obtained through deck-simulation affirm the immense potential of the proposed double barrier AlGaN/AlInGaN/GaN MOSHEMT for future applications in high-power and terahertz frequency domains.

Acknowledgements

This work was supported by the DGRSDT of the ministry of higher education of Algeria.

ORCID

Abderrahim Yousfi, https://orcid.org/0000-0003-2071-728X; **Messai Zitouni,** https://orcid.org/0000-0002-2508-3696
Okba Saidani, https://orcid.org/0000-0003-0507-5581

REFERENCES

[1] M. Haziq, S. Falina, A.A. Manaf, H. Kawarada, and M. Syamsul, "Challenges and Opportunities for High-Power and High-Frequency AlGaN/GaN High-Electron-Mobility Transistor (HEMT) Applications: A Review," Micromachines, **13**, 2133 (2022). https://doi.org/10.3390/mi13122133

[2] B. Mounika, J. Ajayan, S. Bhattacharya, and D. Nirmal, "Recent developments in materials, architectures and processing of AlGaN/GaN HEMTs for future RF and power electronic applications: A critical review," Micro and Nanostructures, **168**, 207317 (2022). https://doi.org/10.1016/j.micrna.2022.207317

[3] S. Xiong, W. Huang, A. Hassan, and R. Zhong, "Simulation study on electrical properties of p-GaN gate normally-off HEMT devices affected by Al mole fraction in AlGaN barrier layer," Journal of Physics: Conference Series, **2355**, 012073 (2022). https://doi.org/10.1088/1742-6596/2355/1/012073

[4] A. Mondal, A. Roy, R. Mitra, and A. Kundu, "Comparative study of variations in gate oxide material of a novel underlap DG MOS-HEMT for analog/RF and high-power applications," Silicon, **12**, 2251-2257 (2020). https://doi.org/10.1007/s12633-019-00316-0

[5] F. Husna, M. Lachab, M. Sultana, V. Adivarahan, Q. Fareed, and A. Khan, "High-Temperature Performance of AlGaN/GaN MOSHEMT with SiO_2 Gate Insulator Fabricated on Si (111) Substrate," IEEE Transactions on Electron Devices, **59**, 2424-2429 (2012). https://doi.org/10.1109/TED.2012.2204888

[6] M. Copel, M. Gribelyuk, and E. Gusev, "Structure and stability of ultrathin zirconium oxide layers on Si (001)," Applied Physics Letters, **76**, 436-438 (2000). https://doi.org/10.1063/1.125779

[7] A. Pérez-Tomás, A. Fontserè, M. Jennings, and P. Gammon, "Modeling the effect of thin gate insulators (SiO_2, SiN, Al_2O_3 and HfO_2) on AlGaN/GaN HEMT forward characteristics grown on Si, sapphire and SiC," Materials science in semiconductor processing, **16**, 1336-1345 (2013). https://doi.org/10.1016/j.mssp.2012.10.014

[8] K. Ahmeda, B. Ubochi, M. Alqaysi, A. Al-Khalidi, E. Wasige, and K.J.M.R. Kalna, "The role of SiN/GaN cap interface charge and GaN cap layer to achieve enhancement mode GaN MIS-HEMT operation," **115**, 113965 (2020). https://doi.org/10.1016/j.microrel.2020.113965

[9] T. Mizutani, M. Ito, S. Kishimoto, and F. Nakamura, "AlGaN/GaN HEMTs with thin InGaN cap layer for normally off operation," **28**, 549-551 (2007). https://doi.org/10.1109/LED.2007.900202

[10] J. Kashiwagi, T. Fujiwara, M. Akutsu, N. Ito, K. Chikamatsu, and K. Nakahara, "Recessed-gate enhancement-mode GaN MOSFETs with a double-insulator gate providing 10-MHz switching operation," **34**, 1109-1111 (2013). https://doi.org/10.1109/LED.2013.2272491

[11] H. Hahn, B. Reuters, A. Wille, N. Ketteniss, F. Benkhelifa, O. Ambacher, H. Kalisch, et al., "First polarization-engineered compressively strained AlInGaN barrier enhancement-mode MISHFET," **27**, 055004 (2012). https://doi.org/10.1088/0268-1242/27/5/055004

[12] N. Ketteniss, L.R. Khoshroo, M. Eickelkamp, M. Heuken, H. Kalisch, R. Jansen, and A. Vescan, "Study on quaternary AlInGaN/GaN HFETs grown on sapphire substrates," **25**, 075013 (2010). https://doi.org/10.1088/0268-1242/25/7/075013

[13] F. Sonmez, E. Arslan, S. Ardali, E. Tiras, E. Ozbay, "Determination of scattering mechanisms in AlInGaN/GaN heterostructures grown on sapphire substrate," Journal of Alloys and Compounds, **864**, 158895 (2021). https://doi.org/10.1016/j.jallcom.2021.158895

[14] P. Murugapandiyan, A. Mohanbabu, V.R. Lakshmi, M. Wasim, and K.M. Sundaram, "Investigation of Quaternary Barrier InAlGaN/GaN/AlGaN Double-Heterojunction High-Electron-Mobility Transistors (HEMTs) for High-Speed and High-Power Applications," J. Electron. Mater. **49**, 524-529 (2020). https://doi.org/10.1007/s11664-019-07731-4

[15] R. Brown, D. Macfarlane, A. Al-Khalidi, X. Li, G. Ternent, H. Zhou, I. Thayne, et al., "A sub-critical barrier thickness normally-off AlGaN/GaN MOS-HEMT," **35**, 906-908 (2014). https://doi.org/10.1109/LED.2014.2334394

[16] M. Khan, J. Kuznia, D. Olson, W. Schaff, J. Burm, and M. Shur, "Deep submicron AlGaN/GaN heterostructure field effect transistors for nficrowave and high temperature applications," in: *52nd Annual Device Research Conference*, Boulder, (CO, USA, 1994), pp. 149-150. https://doi.org/10.1109/DRC.1994.1009451

[17] R. Gaska, M. Shur, T. Fjeldly, and A. Bykhovski, "Two-channel AlGaN/GaN heterostructure field effect transistor for high power applications," Journal of applied physics, **85**, 3009-3011 (1999). https://doi.org/10.1063/1.369621

[18] T.-L. Wu, S.-W. Tang, and H.-J. Jiang, "Investigation of recessed gate AlGaN/GaN MIS-HEMTs with double AlGaN barrier designs toward an enhancement-mode characteristic," Micromachines, **11**, 163 (2020). https://doi.org/10.3390/mi11020163

[19] A.B. Khan, M.J. Siddiqui, and S.G. Anjum, "Comparative study of single and double quantum well AlGaN/GaN HEMT structures for high power GHz frequency application," Materials Today: Proceedings, **4**, 10341-10345 (2017). https://doi.org/10.1016/j.matpr.2017.06.377

[20] D.R. Androse, S. Deb, S.K. Radhakrishnan, and E. Sekar, "T-gate AlGaN/GaN HEMT with effective recess engineering for enhancement mode operation," Materials Today: Proceedings, **45**, 3556-3559 (2021). https://doi.org/10.1016/j.matpr.2020.12.1076

[21] N.M. Shrestha, Y. Li, C.-H. Chen, I. Sanyal, J.-H. Tarng, J.-I. Chyi, and S. Samukawa, et al., "Design and simulation of high-performance lattice matched double barrier normally off AlInGaN/GaN HEMTs," **8**, 873-878 (2020). https://doi.org/10.1109/JEDS.2020.3014252

[22] N.M. Shrestha, C.-H. Chen, Z.-M. Tsai, Y. Li, J.-H. Tarng, and S. Samukawa, "Barrier engineering of lattice matched alingan/gan heterostructure toward high performance e-mode operation," in: *2019 International Conference on Simulation of Semiconductor Processes and Devices (SISPAD)*, (Udine, Italy, 2019), pp. 1-4. https://doi.org/10.1109/SISPAD.2019.8870407

[23] R. Singh, T. Lenka, and H. Nguyen, "T-gate shaped AlN/β-Ga_2O_3 HEMT for RF and high power nanoelectronics," 2021. https://doi.org/10.36227/techrxiv.15023094.v1

[24] S. Dasgupta, D. F. Brown, F. Wu, S. Keller, J.S. Speck, and U.K. Mishra, "Ultralow nonalloyed ohmic contact resistance to self-aligned N-polar GaN high electron mobility transistors by In (Ga) N regrowth," Applied Physics Letters, **96**, 143504 (2010). https://doi.org/10.1063/1.3374331

[25] T. Zine-eddine, H. Zahra, and M. Zitouni, Journal of Science: Advanced Materials and Devices, "Design and analysis of 10 nm T-gate enhancement-mode MOS-HEMT for high power microwave applications," **4**, 180-187 (2019). https://doi.org/10.1016/j.jsamd.2019.01.001
[26] H. Liu, C. Lee, W. Hsu, T. Wu, H. Huang, S. Chen, Y.C. Yang, et al., "AlGaN/GaN MOS-HEMTs with TiO_2 gate dielectric by using non-vacuum ultrasonic spray pyrolysis deposition," in: *2015 IEEE 11th International Conference on Power Electronics and Drive Systems,* 2015, pp. 578-580. https://doi.org/10.1109/PEDS.2015.7203398
[27] H.R. Mojaver, J.-L. Gosselin, and P. Valizadeh, "Use of a bilayer lattice-matched AlInGaN barrier for improving the channel carrier confinement of enhancement-mode AlInGaN/GaN hetero-structure field-effect transistors," Journal of Applied Physics, **121**, 244502 (2017). https://doi.org/10.1063/1.4989836
[28] D. Biswas, H. Fujita, N. Torii, and T. Egawa, "Effect of in composition on electrical performance of AlInGaN/GaN-based metal-insulator-semiconductor high electron mobility transistors (MIS-HEMTs) on Si," **125**, 225707 (2019). https://doi.org/10.1063/1.5098365
[29] T. Nanjo, M. Suita, T. Oishi, Y. Abe, E. Yagyu, K. Yoshiara, and Y. Tokuda, "Comparison of characteristics of AlGaN channel HEMTs formed on SiC and sapphire substrates," **45**, 424-426 (2009). https://doi.org/10.1049/el.2009.0129
[30] M. Gassoumi, A. Helali, H. Maaref, and M. Gassoumi, "DC and RF characteristics optimization of AlGaN/GaN/BGaN/GaN/Si HEMT for microwave-power and high temperature application," Results in Physics, **12**, 302-306 (2019). https://doi.org/10.1016/j.rinp.2018.11.063
[31] A. Yousfi, H. Bencherif, L. Saidi, et al (2018, December). "Role of High-K and gate engineering in improving Rf/analog performances of $In_{0.2}Ga_{0.8}As/Al_{0.3}Ga_{0.7}As$ HEMT," in: *International Conference on Communications and Electrical Engineering (ICCEE)*, (IEEE, 2018), pp. 1-4.
[32] I. Gorczyca, T. Suski, N.E. Christensen, and A. Svane, "Band gap bowing in quaternary nitride semiconducting alloys," Appl. Phys. Lett. **98**, 241905 (2011). https://doi.org/10.1063/1.3597795
[33] O. Ambacher, J. Majewski, C. Miskys, A. Link, M. Hermann, M. Eickhoff, et al., "Pyroelectric properties of Al (In) GaN/GaN hetero- and quantum well structures," Journal of physics: condensed matter, **14**, 3399 (2002). https://doi.org/10.1088/0953-8984/14/13/302
[34] P.K. Kaushik, S.K. Singh, A. Gupta, A. Basu, and E.Y. Chang, "Impact of Surface States and Aluminum Mole Fraction on Surface Potential and 2DEG in AlGaN/GaN HEMTs," Nanoscale Research Letters, **16**, 159 (2021). https://doi.org/10.1186/s11671-021-03615-x
[35] P.-T. Tu, I. Sanyal, P.-C. Yeh, H.-Y. Lee, L.-H. Lee, C.-I. Wu, et al., "Quaternary Barrier AlInGaN/GaN-on-Si High Electron Mobility Transistor with Record F T-L g Product of 13.9 GHz-μm," in: *2020 International Symposium on VLSI Technology, Systems and Applications (VLSI-TSA)*, (IEEE, Piscataway, NJ, USA, 2020), pp. 130-131.
[36] Z.-e. Touati, Z. Hamaizia, and Z. Messai, "DC and RF characteristics of AlGaN/GaN HEMT and MOS-HEMT," in: *Electrical Engineering (ICEE), 2015 4th International Conference* on, (Boumerdes, Algeria, 2015), pp. 1-4. https://doi.org/10.1109/INTEE.2015.7416850
[37] R. Wang, G. Li, J. Verma, B. Sensale-Rodriguez, T. Fang, J. Guo, Z. Hu, et al., "220-GHz quaternary barrier InAlGaN/AlN/GaN HEMTs," **32**, 1215-1217 (2011). https://doi.org/10.1109/LED.2011.2158288
[38] M. Sharma, R. Chaujar, and M. C. A. Engineering, J. I. J. o. R. "Ultrascaled 10 nm T-gate E-mode InAlN/AlN HEMT with polarized doped buffer for high power microwave applications," International Journal of RF and Microwave computer aided engineering, **32**, e23057 (2022). https://doi.org/10.1002/mmce.23057
[39] R. Kajitani, K. Tanaka, M. Ogawa, H. Ishida, M. Ishida, and T. Ueda, "Novel high-current density GaN-based normally off transistor with tensile-strained quaternary InAlGaN barrier," Japanese Journal of Applied Physics, **54**, 04DF09 (2015). https://doi.org/10.7567/JJAP.54.04DF09
[40] J. Jorudas, P. Prystawko, A. Šimukovič, R. Aleksiejūnas, J. Mickevičius, M. Kryśko, P.P Michałowski, et al., "Development of quaternary InAlGaN barrier layer for high electron mobility transistor structures," Materials, **15**, 1118 (2022). https://doi.org/10.3390/ma15031118

ЧИСЛОВЕ ДОСЛІДЖЕННЯ T-GATE AlGaN/AlInGaN/GaN MOSHEMT З ОДИНАРНИМ ТА ПОДВІЙНИМ БАР'ЄРОМ ДЛЯ ЗАСТОСУВАНЬ НА ЧАСТОТІ ТГЦ

Аміна Нуал[a], Мессай Зітуні[b], Зін-Еддін Туаті[b], Окба Сайдані[b], Абдеррахім Юсфі[b]
[a] *Лабораторія LIST, Університет М'Хамед Бугара, Бумердес, Алжир*
[b] *Лабораторія ETA, кафедра електроніки, технологічний факультет, Університет Мохамеда Ель Бачіра Ель Ібрагімі Бордж Бу Арреріджа -34030, Алжир*

У цій статті представлено всебічне дослідження аналогових та змінних мікрохвильових характеристик сучасного Т-образного подвійного бар'єру AlGaN/AlInGaN/GaN MOSHEMT (метал-оксид-напівпровідниковий транзистор з високою мобільністю електронів), реалізованого на підкладці 4H-SiC. Дослідження передбачало ретельне числове моделювання та широке порівняння з проектом одного бар'єру з використанням програмного забезпечення TCAD-Silvaco. Спостережувану різницю в продуктивності можна пояснити використанням технології подвійного бар'єру, яка покращує утримання електронів і щільність струму шляхом збільшення заряду, викликаного поляризацією під час високочастотних операцій. Примітно, що в порівнянні з конструкцією з одним бар'єром подвійний бар'єр MOSHEMT демонструє помітне збільшення струму стоку на 15%, збільшення коефіцієнта провідності на 5% і підвищену напругу пробою (VBR) 140 В у режимі E-mode. Крім того, радіочастотний аналіз подвійного бар'єрного пристрою демонструє виняткову продуктивність, встановлюючи нові рекорди з максимальною частотою коливань (fmax) 1,148 ТГц і граничною частотою підсилення (ft) 891 ГГц. Ці результати, отримані за допомогою дек-симуляції, підтверджують величезний потенціал запропонованого подвійного бар'єру AlGaN/AlInGaN/GaN MOSHEMT для майбутніх застосувань у високопотужних і терагерцевих частотних областях.

Ключові слова: *TiO_2-MOSHEMT; Т-образний затвор; подвійний бар'єр; AlInGaN четвертинний матеріал; максимальна частота ТГц; TCAD-Silvaco*